Physics of Fluids ARTICLE scitation.org/journal/phf

Capillary rise in superhydrophilic rough channels

Cite as: Phys. Fluids 32, 032105 (2020); doi: 10.1063/1.5133826
Submitted: 27 October 2019 • Accepted: 27 February 2020 •
Published Online: 13 March 2020

Jungchul Kim,[1,2] Myoung-Woon Moon,[3] and Ho-Young Kim[1,a)]

AFFILIATIONS

[1] Department of Mechanical and Aerospace Engineering, Seoul National University, Seoul 08826, South Korea
[2] Department of Thermal Systems, Korea Institute of Machinery & Materials, Daejeon 34103, South Korea
[3] Computational Science Research Center, Korea Institute of Science and Technology, Seoul 02792, South Korea

[a)] **Author to whom correspondence should be addressed:** hyk@snu.ac.kr

ABSTRACT

Surface tension forces enable a liquid to rise against gravity when wettable tubes or porous media are in contact with the pool of liquid. While the rise dynamics in the media of homogeneous porosity are well known, those in heterogeneous porous media still remain poorly understood. Here, we employ a vertical channel formed by two parallel plates decorated with micropillars, as a simple model of bidisperse porous media, and observe the rise dynamics of various viscous liquids. We find the bulk rise speed to be higher than that in dry smooth channels but equal to that between prewetted smooth channels. As the bulk approaches its equilibrium height, a film emerges ahead of the bulk meniscus, which is driven by the high surface energy of the microdecorated surface. The film extension grows initially like t but later like $t^{1/2}$, with t being time. We construct theoretical models to predict the critical height where the film emerges and to rationalize the power laws of the film extension. In particular, we show that the dominant viscous resistance to the film extension is provided by the flow from the reservoir through the bulk in the early stages and by the film itself in the late stages. Our study opens a pathway to scrutinize the complicated flow dynamics arising within and across voids of heterogeneous porous media with an easily observable experimental setup of a well-defined geometry.

I. INTRODUCTION

In the early eighteenth century, Jurin studied the dependence of the rise height of a liquid within a wettable circular capillary upon liquid properties and tube diameter.[1] Although the equilibrium height of a liquid column, or Jurin's height, in a smooth hydrophilic capillary is easily obtained by balancing the upward surface tension force and the downward gravitational force,[2] the dynamics of the rise have been the subject of intensive study over centuries. Neglecting the effects of inertia for a viscous flow into a long thin tube, the Poiseuille flow assumption adopting the driving pressure that decreases with the rise height gives the average flow rate. The analysis for a single tube is frequently extended to porous media with uniformly sized voids, which are modeled as an assemblage of identical tubes.[3]

The capillary rise in porous media with heterogeneous sizes of voids, such as cellulose sponges,[4,5] rocks,[6–8] paper,[9] fabrics,[10] and polymer membranes,[11] is more complicated than the rise in the media of uniform pores because the pore size determines the magnitudes of both the capillary driving force and viscous resisting force. Using a horizontally situated compound capillary, where a small fiber was introduced into a larger tube, it was shown that liquids wick faster along the interstice than in the large tube.[12] The liquid rising in cellulose sponges against gravity was found to completely fill both the macro- and microscale voids in the early stages but partially fill the macroscale voids beyond a critical elevation.[4,5] Despite the previous findings that the capillary rise can arise at different rates in voids of different sizes within a single porous medium, the direct visualization of flow bifurcation, and the measurement and analysis of those compound rise dynamics in a controlled geometry are yet to be achieved. Here, we employ a model system where two distinct sizes of pores (bidisperse porosity) are provided by microdecorating inner walls of millimetric channels consisting of two parallel plates, as shown in Fig. 1.

Modeling porous media of bidisperse porosity using tubes of microdecorated inner surface were suggested earlier,[13] although major interest of the work was on the wetting states of single rough surfaces. It was predicted that the film invading the microtexture

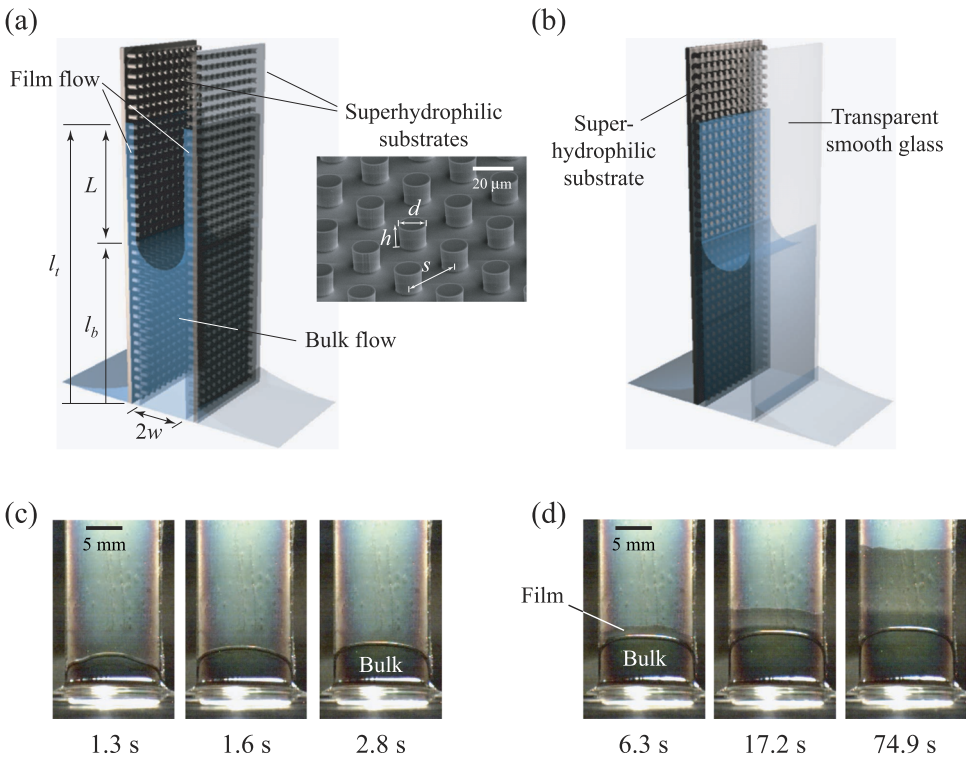

FIG. 1. (a) Schematic of the liquid rise between superhydrophilic sheets. The SEM (scanning electron microscopy) image shows the micropillar array. (b) An auxiliary setup allowing for clear visualization of the bulk and film flows. (c) The rise of the bulk of liquid A in the early stages. (d) The film spreading ahead of the bulk in the late stages. The pillar height, diameter, and spacing are 35 μm, 20 μm,, and 40 μm, respectively, and the gap between the plates is 0.6 mm.

would propagate faster than the bulk in the tube. The spreading of the liquid on a horizontally situated superhydrophilic surface was investigated,[14–16] revealing different power laws of wet distance l vs time t depending on the source strength. The rise dynamics of a liquid film on a vertically situated single superhydrophilic substrate were studied,[17] to find that the microscopic zippering of the liquid front accumulates to lead to the diffusive dynamics of a macroscopic rise height, $l \sim t^{1/2}$.

In this work, we observe and measure the vertical rise of a liquid in microdecorated (bidisperse porosity) channels and elucidate the difference of the dynamics from those in smooth channels (monodisperse porosity). In addition, we construct scaling laws to explain the salient feature of our system, i.e., the wicking of the liquid film ahead of the bulk in the late stages. Our simple experimental model system with controlled sizes of pores opens a pathway to a detailed understanding of the wicking dynamics in media of heterogeneous porosity.

II. EXPERIMENTAL

As a two-dimensional channel with highly wettable rough inner surfaces, we use two parallel Si wafers decorated with cylindrical micropillar arrays fabricated by the deep reactive ion etching process. The diameter d and height h of the pillars in a square array with pitch s, as shown in Fig. 1(a), are varied by the design of the photomask and the etching duration. In our experiments, d and h vary from 10 μm to 20 μm and from 2.7 μm to 35 μm, respectively, while s is fixed to be 40 μm. The pillars are arrayed with no skewness, implying that the liquid propagation arises in the same direction as the vertical alignment of the pillars.[17] The pillar arrays are coated with a Si-incorporated diamond-like carbon film and then etched with air plasma to turn superhydrophilic, owing to the hydrophilic Si–O bonds and nanoscale roughness. For more detailed process conditions, see Yi *et al.*[21]

As liquids, we use aqueous glycerine 90 wt. % and 85 wt. %, a mixture of ethylene glycol (EG) and glycerine, silicone oils 350 cSt and 1000 cSt, whose surface tension γ, viscosity μ, and density ρ are listed in Table I. All the liquids wet smooth plasma-treated silicon surfaces with the equilibrium contact angles being nearly 5° as measured by drawing a tangential line to the liquid–air interface of sessile drops of 100 μl volume. The gap between the parallel plates, $2w$, varies from 0.45 mm to 1.19 mm. The width of each plate is 14 mm. The rise of the liquid is recorded with a CMOS (complementary metal oxide semiconductor) camera with a frame rate of 30 s^{-1} or 60 s^{-1}.

When the lower end of the channel formed by the parallel plates touches a liquid, the liquid rises into the gap, as shown in Fig. 1. Only a bulk is observed in the early stages. However, distinct from classical experiments with smooth channel walls, a film emerges ahead of the bulk in the late stages, where the bulk hardly rises due to the gravitational effects. Although it is possible to track the height of the bulk rising between opaque Si plates by observing the channel side, the quantitative measurement of film propagation from the side is nearly impossible. Thus, we employ an auxiliary experimental setup where one of the walls is replaced by a prewetted transparent smooth glass slide, as shown in Fig. 1(b), which

TABLE I. Properties of liquids measured at 25 °C. EG stands for ethylene glycol.

	Liquid	Surface tension (N m^{-1})	Viscosity (Pa s)	Density (kg m^{-3})
A	Glycerine 90 wt. %	0.063	0.125	1225
B	Glycerine 85 wt. %	0.063	0.086	1213
C	EG 60 wt. %–Glycerine 40 wt. %	0.052	0.062	1168
D	Silicone oil 350 cSt	0.020	0.35	970
E	Silicone oil 1000 cSt	0.020	1.00	970

greatly facilitates the visualization of the film. It was confirmed that both the channels (two rough walls vs one smooth and one rough wall) exhibit an identical bulk rise speed. The film flow on a rough wall is naturally assumed to arise independent of the condition of the other wall. The liquid can rise via two paths when touching superhydrophilic channels. That is, the rise may occur through the large spacing of the parallel plates (the bulk flow) and through the gaps of micropillars (the film flow). We analyze the rise rates of the two flows and compare the theoretical results with the experimental observations.

III. RISE DYNAMICS OF THE BULK

The rise speed of the bulk between parallel plates whose width is much greater than the gap is given by the average velocity of the two-dimensional Poiseuille flow,

$$\dot{l}_b = \frac{w^2 \Delta p}{3\mu l_b}, \tag{1}$$

where l_b is the rise height of the bulk, $\dot{l}_b = \mathrm{d}l_b/\mathrm{d}t$ with t being the time, and the pressure difference $\Delta p = \gamma/w - \rho g l_b$ with g being the gravitational acceleration.[2] This inertia-free model is valid except at the beginning of the rise, whose characteristic time scale $\tau = \rho w^2/\mu \sim 10^{-4}$ or 10^{-3} s in our experiments. In the initial stages where the gravitational effect is insignificant as compared with the capillary effect, i.e., $\Delta p = \gamma/w$, the rise height follows the classical rule of Washburn:[3,22,23] $l_b \approx (D_b t)^{1/2}$, where the dynamical coefficient for the initial bulk flow $D_b = 2\gamma w/(3\mu)$.

The flow of the liquid film through the gaps of micropillar arrays is termed hemiwicking,[17] whose front propagation, l_f, arises as driven by the capillary force and resisted by the viscous shear force. Hemiwicking in general yields the diffusive behavior of l_f: $l_f = (D_f t)^{1/2}$ with D_f corresponding to the dynamical coefficient.[17–20] We take the model of Ref. 17, which was shown to be valid for a wide range of micropillar array dimensions. In the model, the capillary and viscous forces per unit width are, respectively, scaled as $(f-1)\gamma$ and $\mu \dot{l}_f l[h^{-1} + (f-1)/s]$, where f is the roughness defined as the ratio of the actual surface area to the projected area. For detailed derivation of the theory, readers are referred to Ref. 17. Balancing the driving and resisting forces in view of negligible inertia gives $D_f = k_f \gamma \eta h/\mu$ with $k_f = 0.24$ being the empirically determined coefficient valid for all microdecorated surfaces and $\eta = (f-1)/[1 + h(f-1)/s]$.[17]

As both the bulk and film flows exhibit diffusive dynamics, we consider the ratio of their dynamical coefficients, D_b/D_f, which can be scaled as $w/(\eta h)$. As η is of the order of unity in our experiments, the flows through large pores dominate the initial wicking dynamics when the sizes of the large and small pores are far apart: $w/h \gg 1$. It is the case in our experiments where $w/h \sim 10^2$, consistent with the experimental finding that only the bulk is observed through the camera in Fig. 1(c). We note that the bulk hardly rises due to gravitational effects in the late stages, where the film emerges leaving the slow and then stationary bulk behind, a topic of Sec. IV.

Now a question naturally arises whether the superhydrophilic walls enhance the rise speed of the bulk. Thus, we experimentally compared the rise height in the rough superhydrophilic channel with that in smooth hydrophilic channels. As smooth channel surfaces, we used both dry and prewetted ones. For dry channels, the glass slides were cleaned by using a piranha solution for 1 h to turn highly wettable and then completely dried by nitrogen gas. For prewetted channels, the piranha cleaned glass slides were dip-coated by liquid A with a thickness of approximately 10 μm.

Figure 2(a) shows the experimentally measured height of the bulk of liquid A vs time for different channel surface conditions. Here, the rise height l_b is scaled by the equilibrium capillary rise height between parallel plates with a zero contact angle, or Jurin's height, $l_J = \gamma/(\rho g w)$. The height is measured in the middle of the interface, where the edge effects extending by the order of the capillary length, $[\gamma/(\rho g)]^{1/2}$, are diminished and the two-dimensional interface assumption is satisfied. We see that the rise in the dry smooth channel is slower and stops earlier than the other cases. It is because, on initially dry surfaces, the dynamic contact angle (θ_A) of the rapidly advancing contact line is relatively large,[24,25] which lowers the driving capillary pressure to $2\gamma \cos\theta_A/w$ from $2\gamma/w$. In addition, the movements of contact lines on dry surfaces experience greater resistance than those on prewetted surfaces.[26] The slower rise of the bulk in a channel formed by dry smooth surfaces implies that precursor films of molecular or nanoscopic scales that may be present ahead of macroscopic contact lines[27] play insignificant roles compared with microprotrusions or prewetted films, in determining the macroscopic wetting speeds.

The liquid rise in the initially dry superhydrophilic rough channels occurs much faster than that in the initially dry smooth channel so that the rate is comparable to that in prewetted smooth channels. It indicates that the apparent advancing contact angle of the bulk meniscus in the superhydrophilic channel is nearly zero and that the bulk meniscus moves on a liquid filling the gaps of micropillars. Therefore, the curvature of the liquid–gas interface of the bulk becomes $1/w$ and the resistance to the meniscus movement is less than that on dry smooth surfaces.

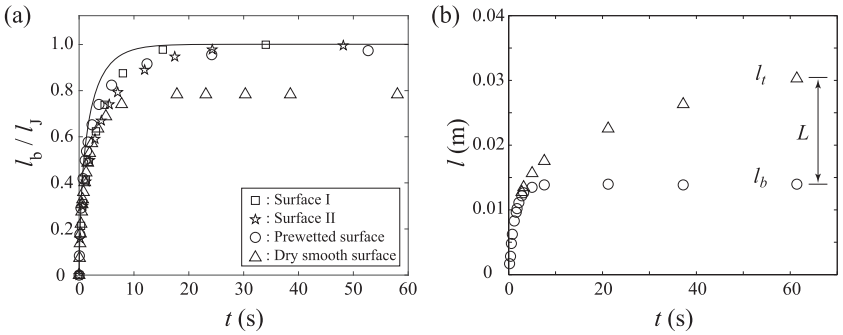

FIG. 2. (a) The rise height of the bulk of liquid A within a dry smooth channel, a prewetted smooth channel, and dry superhydrophilic rough channels with a gap of $2w$ = 0.6 mm. The pillar dimensions of the micropillared surfaces are such that [d, h] = [10, 25] and [20, 2.7] μm for surfaces I and II, respectively. The solid line corresponds to the theoretical prediction assuming the Poiseuille flow from the beginning, which tends to overestimate the initial rise speed. (b) The measurement results of the meniscus height vs time, corresponding to Figs. 1(c) and 1(d). Error bars are smaller than symbols.

Before we move on to the film flows in the late stages, we consider the effects of the spacing between plates, $2w$, on the bulk dynamics. The initially dry and prewetted smooth plates were held apart at the same distance, meaning that the actual spacing for the prewetted channel is approximately 20 μm smaller than that of the dry smooth channel due to the liquid films. The spacing of pillared surfaces denotes the distance between the tops of pillars of two facing surfaces. Because the plate spacing, ranging from 0.45 mm to 1.19 mm, is much greater than the liquid film thickness on the prewetted surface (10 μm) and the pillar height (3–35 μm), the slight change of the plate spacing either due to the prewetting liquid film or pillars exerts negligible effects on our bulk rise experiments.

IV. EMERGENCE OF THE FILM

The microdecorated hydrophilic surface with a very high surface energy per projected area tends to attract a liquid film to lower its energy state. Therefore, as the rise speed of the bulk decreases with its height approaching the equilibrium rise height, l_J, a visible film emerges, as shown in Fig. 1(d). Such a transition of the rise dynamics occurs at the critical height, l_c, where the film spreading speed dominates over the bulk rise speed. In this initial period of film emergence, the film has not wetted the entire height of pillars lying ahead of the bulk yet. Rather, it extends from the bulk meniscus to the front contact line in a wedge-like shape, as shown in Fig. 3(a).

The pressure difference between the wedge meniscus and the atmosphere owing to capillarity is scaled as $(f\cos\theta - 1)\gamma/h$, a result of scaling the capillary force per unit width as $(f\cos\theta - 1)\gamma$,[17] with θ being the contact angle of the wedge meniscus. For $\theta \ll 1$ and $\cos\theta \approx 1$, we approximate the pressure drop as $(f-1)\gamma/h$. Because the capillary pressure jump established between the bulk meniscus and the atmosphere is γ/w, the pressure difference between the bulk and the film is scaled as $(f-1)\gamma/h$ for $h \ll w$. Thus, the driving force per unit width of the emergence of the film is scaled as $F_d \sim (f-1)\gamma$. The viscous shear stress acting on the wedge with a low contact angle, $\theta \approx 5^\circ$, is estimated as $\tau_w \approx \mu\dot{l}_t/(x\theta)$, where $\dot{l}_t$ is the film propagation speed near the critical height l_c and x is the distance from the contact line, as indicated in Fig. 3(a). We note again that θ is the contact angle of the front wedge of the film, not the angle that determines the curvature of the bulk meniscus. The shear force on the rough area is scaled as $F_r \sim \int_\lambda^\Lambda \tau_w f \mathrm{d}x \sim \mu\dot{l}_t f\Gamma/\theta$, where Λ is the characteristic extension of the wedge, λ is the cutoff length introduced to relieve the contact line singularity,[26] and $\Gamma = \ln(\Lambda/\lambda)$. Balancing the driving capillary force, F_d, and the resisting viscous force, F_r, yields the scaling estimate of the emergence speed of the liquid wedge,

$$\dot{l}_t \sim \frac{\gamma\phi\theta}{\mu\Gamma}, \tag{2}$$

where $\phi = 1 - 1/f$.

The critical height for the emergence of the film from the bulk is then obtained by taking $\dot{l}_b \sim \dot{l}_t$. Substituting l_c for l_b in Eq. (1), we find

$$\frac{l_c}{l_J} = \frac{1}{1 + k\phi\theta l_J/w}, \tag{3}$$

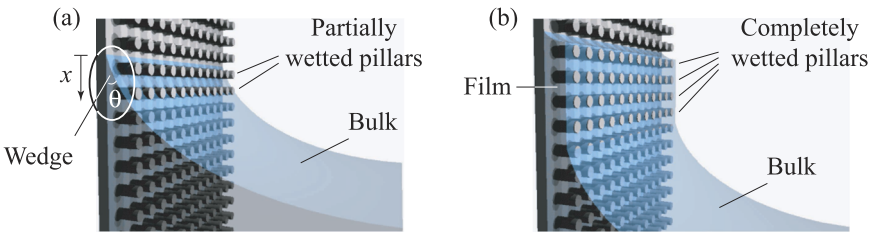

FIG. 3. (a) Schematic of the meniscus wedge of a visible film that significantly emerges from the bulk but partially wets the micropillars ahead of the bulk. (b) The film extending from the bulk by completely wetting the micropillars ahead of the bulk.

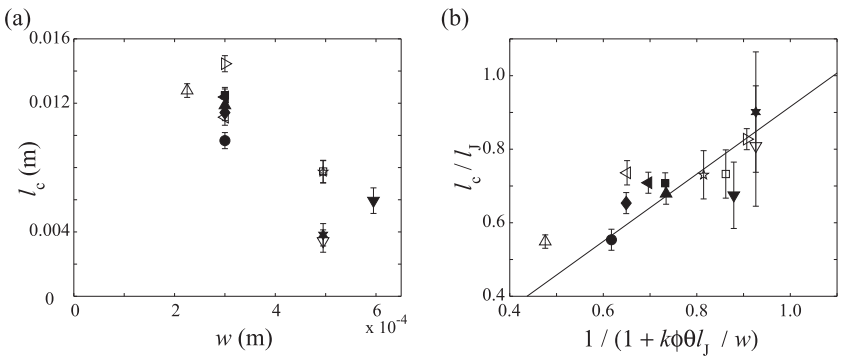

FIG. 4. (a) The critical height at which the film emerges, l_c, vs w. (b) The scaled critical height l_c/l_J plotted according to the scaling law (3). Here, we used the experimentally measured value of $\theta = 5°$, and the empirical constant k was found to be 0.21 through the least squares method. Experimental conditions for the symbols are listed in Table II. The length of error bars corresponds to the range of the bulk height where the film flow becomes gradually clear.

TABLE II. Experimental conditions for the symbols in Figs. 4 and 5. In the last column, ϵ is the experimental uncertainty in the measurement of l_c.

Symbol	Liquid	$2w$ (mm)	s (μm)	d (μm)	h (μm)	f	l_c (mm)	ϵ/l_J
△	A	0.45	40	20	35	2.37	12.8	0.0182
▲	A	0.60	40	10	26	1.51	11.9	0.0286
◂	A	0.60	40	10	35	1.69	12.4	0.0286
▷	A	0.60	40	20	5	1.10	14.5	0.0286
♦	A	0.60	40	20	26	2.02	11.4	0.0286
●	A	0.60	40	20	35	2.37	9.68	0.0286
□	A	0.99	40	10	35	1.69	7.76	0.0656
☆	A	0.99	40	20	35	2.37	7.74	0.0656
▼	A	1.19	40	20	26	2.02	5.94	0.0902
■	B	0.60	40	10	26	1.51	12.5	0.0283
◁	C	0.60	40	20	35	2.37	11.1	0.0331
★	D	0.99	40	20	26	2.02	3.83	0.164
▽	E	0.99	40	20	26	2.02	3.43	0.164

where k is a prefactor to be determined empirically. We plot experimental measurement results of l_c vs w in Fig. 4(a), whose experimental conditions are listed in Table II. Figure 4(b) shows that the scattered data in (a) are collapsed onto a single line when plotted according to our scaling law (3). Our theory and experiments on the film emergence reveal that the critical height increases with Jurin's height, corresponding to the relatively high rise velocity of the bulk. But, l_c decreases with the roughness because of the enhanced speed of the film. When the plate is smooth, or $f \to 1$ and $\phi \to 0$, we get $l_c \to l_J$ corresponding to nearly no film emergence.

V. RISE DYNAMICS OF THE FILM

Once the visible film starts to emerge from the bulk, the area wetted by the film continues to grow, whose vertical extension is measured by $L = l_t - l_b$. To find the extension rate of the film, we first consider the change of the bulk flow rate owing to the film propagation at the advancing front. When only the bulk flow is to be seen, the average velocity within the bulk, U is naturally $U = \dot{l}_b$. However, with the advent of the film ahead, we write the continuity relation as $U(w+\beta_1 h) = \dot{l}_b w + \beta_2 \dot{L} h$, where the left-hand side corresponds to the flow rate behind the meniscus and the right-hand side is the sum of the advancing flow rates of the bulk and film. Here, β_1 and β_2 denote the effective flow passage ratio through the gaps of micropillars.[28–30] Using $w \gg h$, U is simplified to $U \approx \dot{l}_b + \beta_2 h\dot{L}/w$, implying that the liquid flow rate pumped to the advancing front is increased due to the film flow. The dominant flow path from the bulk to the film is indicated in Fig. 5(a).

The conservation of energy states that the decrease rate of surface energy is balanced by the rates of viscous energy dissipation and increase in gravitational potential energy. As the liquid climbs the channel, the surface energy decrease rate associated with the bulk rise is given by $\dot{E}_b = \gamma \dot{l}_b$ and that with the film rise by $\dot{E}_s = (f-1)\gamma \dot{l}_t$.[17] The viscous dissipation associated with the bulk rise is scaled as $\mu U \dot{l}_b l_b / w$, which can be decomposed into the original contribution of the bulk flow, $\Phi_o \sim \mu \dot{l}_b^2 l_b / w$, and the additional term owing to the

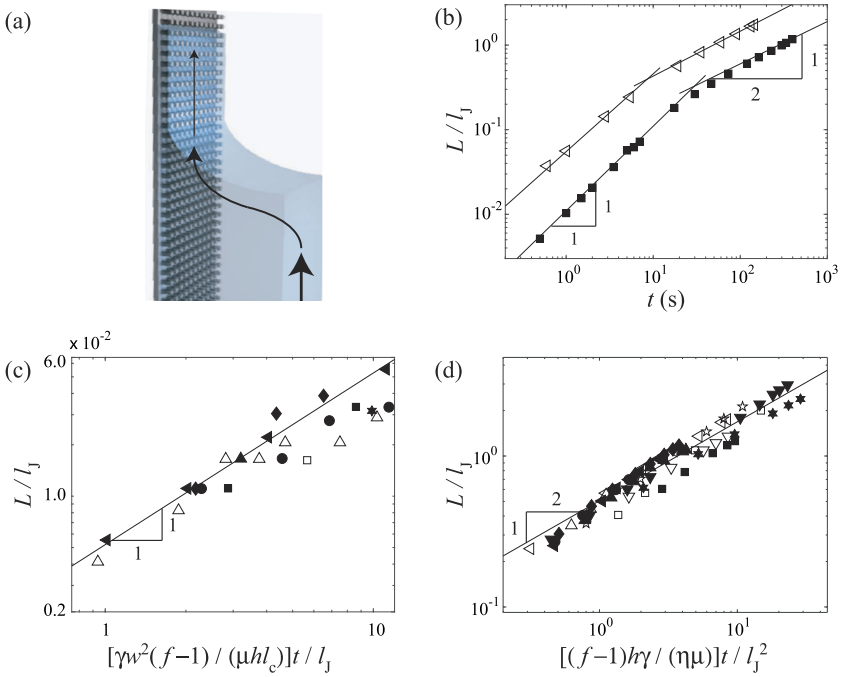

FIG. 5. (a) A schematic of the dominant flow path from the bulk to the film. (b) Representative measurement results of the film extension, $L = l_t - l_b$, vs time whose zero indicates the moment the film begins to be visible. (c) Scaled film extension, L/l_J, plotted according to Eq. (4), which is valid for the early stages. (d) Scaled film extension, L/l_J, plotted according to Eq. (5), which is valid for the late stages. The symbols correspond to those in Table II, and they are larger than error bars.

film flow ahead, $\Phi_a \sim \mu l_b(U-\dot{l}_b)\dot{l}_b/w$. The viscous dissipation within the film is scaled as $\Phi_f \sim \mu\eta L\dot{L}\dot{l}_t$. The gravitational energy increase rate is $\Phi_g = \rho g w l_b \dot{l}_b$ with a negligible contribution of the film.

Besides the energy change rates responsible for the classical bulk rise ($\dot{E}_b = \Phi_o + \Phi_g$), the following balance describes the film dynamics: $\dot{E}_s = \Phi_a + \Phi_f$. Comparison of the magnitudes of Φ_a and Φ_f leads us to consider two regimes. When $\Phi_a \gg \Phi_f$, corresponding to $L/l_J \ll (h/w)^2$ or relatively small extension of the film in the early stages of the film flow, $\dot{E}_s \sim \Phi_a$ yields

$$L \sim (f-1)\frac{\gamma}{\mu}\frac{w^2}{hl_c}t. \tag{4}$$

When $\Phi_a \ll \Phi_f$ or in the late stages with a relatively large L, we recover the same expression as the hemiwicking film from the stationary liquid reservoir,[17]

$$L \sim \left[\frac{(f-1)}{\eta}\frac{\gamma}{\mu}\right]^{1/2} t^{1/2}. \tag{5}$$

The film extension is theoretically predicted to grow like t in the early stages but to grow diffusively in the late stages, which is, indeed, observed experimentally in Fig. 5(b). In the early stages, the dominant viscous dissipation associated with the film propagation occurs in the bulk flow to supply the liquid from the liquid reservoir to the film. As the film area grows in the late stages, the viscous dissipation in the film itself becomes dominant. The effects of the bulk flow on the film flow in the early stages are manifested by the parameters related to the bulk flow, w and l_c, in Eq. (4), while they are absent in Eq. (5) for the late stages.

The two scaling laws, (4) and (5), are shown to explain the film extensions of various experimental conditions. Figure 5(c) shows that the experimental data in the early stages of the film flow are collapsed onto a single line when plotted according to Eq. (4), but they deviate from the scaling law before L/l_J reaches 10^{-1}. In the late stages, Eq. (5) collapses the experimental data onto a single line, validating our theory, as shown in Fig. 5(d).

VI. CONCLUSIONS

We have experimentally observed the capillary rise dynamics within channels formed by microdecorated hydrophilic surfaces, to find the emergence of the film flow ahead of the bulk as Jurin's height is approached. The initial bulk rise speed is higher than that in dry smooth channels, but rather identical to that in prewetted smooth channels. This allows us to assume that the bulk meniscus is formed around a liquid film occupying the gaps of micropillars to make the meniscus curvature and contact line resistance similar to those in prewetted smooth channels. The visible film ahead of the bulk emerges when the advancing speed of the front wedge through the micropillars dominates over the bulk rise rate. The extension of the film from the bulk meniscus is found to grow like t initially and then like $t^{1/2}$ in the late stages. This is because the viscous dissipation arises dominantly by the flow through the bulk from the reservoir in the early stages but the dissipation is dominated by the flow of the film itself in the late stages.

We have employed the millimetric gaps between microdecorated plates as a simple model of bidisperse porous media with a well-defined geometry. The experimental results obtained using this model are consistent with previous heterogeneous porous media in that the capillary rise dynamics are governed by the bulk rise initially but by film flows in the late stages.[4,5] Although our system adopting parallel plates enables us to scrutinize the dynamics of the film from its emergence to growth, the interaction of

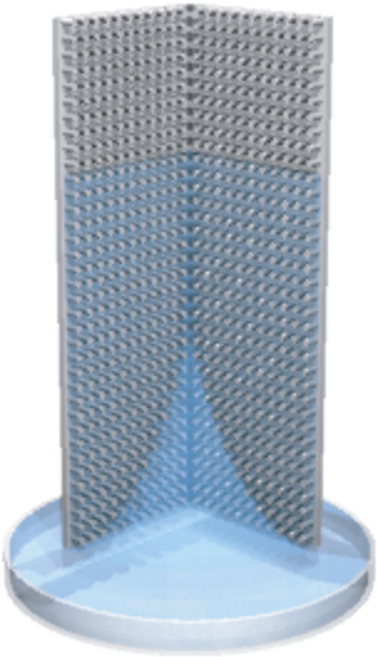

FIG. 6. A schematic of a simple model of channels with heterogeneous pores involving corners of two microdecorated surfaces.

macroscale and microscale voids ceases beyond the critical height, l_c. However, such interaction persists as a liquid wicks into corners of macroscale voids in such porous media as sponges,[4,5] while it is excluded in our current setting. Therefore, next evolution of our system to help the understanding of complicated real porous flows would involve devising corners of macroscale voids, as illustrated in Fig. 6. Visualizing the interaction of corner flows, which become narrower upstream,[31,32] with neighboring superhydrophilic micropillars would more clearly elucidate the inter-pore flow dynamics occurring in the capillary rise of heterogeneous porous media.

ACKNOWLEDGMENTS

This work was supported by the National Research Foundation of Korea (Grant No. 2018-052541) and Ministry of Trade, Industry and Energy of Korea (Grant No. 2018-20000187) via SNU-IAMD.

REFERENCES

[1]J. Jurin, "II. An account of some experiments shown before the Royal Society; with an enquiry into the cause of the ascent and suspension of water in capillary tubes," Philos. Trans. R. Soc. London **30**, 739–747 (1718).
[2]R. F. Probstein, *Physicochemical Hydrodynamics: An Introduction*, 2nd ed. (Wiley, Hoboken, NJ, 2013).
[3]E. W. Washburn, "The dynamics of capillary flow," Phys. Rev. **17**, 273–283 (1921).
[4]J. Kim, J. Ha, and H.-Y. Kim, "Capillary rise of non-aqueous liquids in cellulose sponges," J. Fluid Mech. **818**, R2 (2017).
[5]J. Ha, J. Kim, Y. Jung, G. Yun, D.-N. Kim, and H.-Y. Kim, "Poro-elasto-capillary wicking of cellulose sponges," Sci. Adv. **4**, eaao7051 (2018).
[6]S. F. Nia and K. Jessen, "Theoretical analysis of capillary rise in porous media," Transp. Porous Media **110**, 141–155 (2015).
[7]I. Jafari, M. Masihi, and M. N. Zarandi, "Numerical simulation of counter-current spontaneous imbibition in water-wet fractured porous media: Influences of water injection velocity, fracture aperture, and grains geometry," Phys. Fluids **29**, 113305 (2017).
[8]Q. Gu, L. Zhu, Y. Zhang, and H. Liu, "Pore-scale study of counter-current imbibition in strongly water-wet fractured porous media using lattice Boltzmann method," Phys. Fluids **31**, 086602 (2019).
[9]M. Lee, S. Kim, H.-Y. Kim, and L. Mahadevan, "Bending and buckling of wet paper," Phys. Fluids **28**, 042101 (2016).
[10]S. J. Kim, J. W. Choi, M.-W. Moon, K.-R. Lee, Y. S. Chang, D.-Y. Lee, and H.-Y. Kim, "Wicking and flooding of liquids on vertical porous sheets," Phys. Fluids **27**, 032105 (2015).
[11]R. L. Thankamony, X. Li, X. Fan, G. Sheng, X. Wang, S. Sun, X. Zhang, and Z. Lai, "Preparation of highly porous polymer membranes with hierarchical porous structures via spinodal decomposition of mixed solvents with UCST phase behavior," ACS Appl. Mater. Interfaces **10**, 44041–44049 (2018).
[12]J. Bico and D. Quéré, "Precursors of impregnation," Europhys. Lett. **61**, 348–353 (2003).
[13]J. Bico, U. Thiele, and D. Quéré, "Wetting of textured surfaces," Colloids Surf., A **206**, 41–46 (2002).
[14]S. J. Kim, M.-W. Moon, K.-R. Lee, D.-Y. Lee, Y. S. Chang, and H.-Y. Kim, "Liquid spreading on superhydrophilic micropillar arrays," J. Fluid Mech. **680**, 477–487 (2011).
[15]S. J. Kim, J. Kim, M.-W. Moon, K.-R. Lee, and H.-Y. Kim, "Experimental study of drop spreading on textured superhydrophilic surfaces," Phys. Fluids **25**, 092110 (2013).
[16]J. Kim, M.-W. Moon, K.-R. Lee, L. Mahadevan, and H.-Y. Kim, "Hydrodynamics of writing with ink," Phys. Rev. Lett. **107**, 264501 (2011).
[17]J. Kim, M.-W. Moon, and H.-Y. Kim, "Dynamics of hemiwicking," J. Fluid Mech. **800**, 57 (2016).
[18]J. Bico, C. Tordues, and D. Quéré, "Rough wetting," Europhys. Lett. **55**, 214 (2001).
[19]L. Courbin, E. Denieul, E. Dressaire, M. Roper, A. Ajdari, and H. A. Stone, "Imbibition by polygonal spreading on microdecorated surfaces," Nat. Mater. **6**, 661 (2007).
[20]C. Ishino, M. Reyssat, E. Reyssat, K. Okumura, and D. Quéré, "Wicking within forests of micropillars," Europhys. Lett. **79**, 56005 (2007).
[21]J. W. Yi, M.-W. Moon, S. F. Ahmed, H. Kim, T.-G. Cha, H.-Y. Kim, S.-S. Kim, and K.-R. Lee, "Long-lasting hydrophilicity on nanostructured Si-incorporated diamond-like carbon films," Langmuir **26**, 17203–17209 (2010).
[22]J. M. Bell and F. K. Cameron, "The flow of liquids through capillary spaces," J. Phys. Chem. **10**, 658–674 (1906).
[23]R. Lucas, "Uber das zeitgesetz des kapillaren aufstiegs von flussigkeiten," Kolloid-Z. **23**, 15–22 (1918).
[24]R. L. Hoffman, "A study of the advancing interface. I. Interface shape in liquid-gas systems," J. Colloid Interface Sci. **50**, 228–241 (1975).
[25]G. Ström, M. Fredriksson, P. Stenius, and B. Radoev, "Kinetics of steady-state wetting," J. Colloid Interface Sci. **134**, 107–116 (1990).
[26]P. G. de Gennes, "Wetting: Statics and dynamics," Rev. Mod. Phys. **57**, 827–863 (1985).
[27]D. Bonn, J. Eggers, K. Indekeu, J. Meunier, and E. Rolley, "Wetting and spreading," Rev. Mod. Phys. **81**, 739–805 (2009).
[28]A. V. Kuznetsov, "Analytical investigation of the fluid flow in the interface region between a porous medium and a clear fluid in channels partially filled with a porous medium," Appl. Sci. Res. **56**, 53–67 (1996).
[29]R. Bavière, G. Gamrat, M. Favre-Marinet, and S. Le Person, "Modeling of laminar flows in rough-wall microchannels," J. Fluids Eng. **128**, 734–741 (2006).
[30]A. Lee and H.-Y. Kim, "Does liquid slippage within a rough channel always increase the flow rate?," Phys. Fluids **26**, 072002 (2014).
[31]A. Ponomarenko, D. Quéré, and C. Clanet, "A universal law for capillary rise in corners," J. Fluid Mech. **666**, 146–154 (2011).
[32]M. M. Weislogel, "Compound capillary rise," J. Fluid Mech. **709**, 622–647 (2012).